Effects of Temperature and Particle Size on Deposition in Land Based Turbines

Jared M. Crosby

Scott Lewis

Jeffrey P. Bons

Department of Mechanical Engineering,
Brigham Young University,
Provo, UT 84602

Weiguo Ai

Thomas H. Fletcher

Department of Chemical Engineering,
Brigham Young University,
Provo, UT 84602

Four series of tests were performed in an accelerated deposition test facility to study the independent effects of particle size, gas temperature, and metal temperature on ash deposits from two candidate power turbine synfuels (coal and petcoke). The facility matches the gas temperature and velocity of modern first stage high pressure turbine vanes while accelerating the deposition process. Particle size was found to have a significant effect on capture efficiency with larger particles causing significant thermal barrier coating (TBC) spallation during a 4 h accelerated test. In the second series of tests, particle deposition rate was found to decrease with decreasing gas temperature. The threshold gas temperature for deposition was approximately 960°C. In the third and fourth test series, impingement cooling was applied to the back side of the target coupon to simulate internal vane cooling. Capture efficiency was reduced with increasing mass flow of coolant air; however, at low levels of cooling, the deposits attached more tenaciously to the TBC layer. Postexposure analyses of the third test series (scanning electron microscopy and X-ray spectroscopy) show decreasing TBC damage with increased cooling levels. [DOI: 10.1115/1.2903901]

Keywords: deposition, syngas, turbines

Introduction

The effects of solid particles ingested into gas turbines are a universal problem shared by both land based and aircraft turbines. Due to the large air flow that gas turbines require, these particles cannot economically be entirely eliminated from the inlet air flow even with the best filtration and cleanup systems. Internal particulate sources include combustion products of fossil fuels, eroded turbomachinery components, and secondary chemical reactions. External particulate sources vary widely depending on operating environment (marine, desert, and industrial) and level of filtration (aeroengine, remote power microturbine, or large industrial power plant). These contaminants are heated in the combustor and either follow the flow out of the engine or impact against the turbine blades, which results in erosion, corrosion, and deposition. Erosion and deposition are competing phenomena and depend on the phase of the particulate impacting the blade surfaces. While there are numerous secondary parameters influencing these processes, generally the particulate erodes the blades when it is below the softening temperature and adheres to the blades when above the softening temperature. This threshold temperature depends on the particulate type, but has been shown to occur between 980°C and 1150°C [1–5].

The primary factors affecting the extent of deposition on turbine blades include gas temperature, turbine surface temperature, net particle loading, particulate chemical composition, turbine blade exposure time, and geometric boundaries imposed on the flow. Previous turbine tests with coal-derived fuels by Wenglarz and Fox [4] show a dramatic increase in deposition rate as the gas temperature is raised above the particulate melting point. In their study, coated turbine superalloy specimens were subjected to 2–5 h of deposition from three coal-water fuel (CWF) formulations. The coal had been cleaned to simulate ash levels (~1%) that would be considered acceptable for use in a gas turbine. The fuel was burned in a low-emission subscale turbine combustor at realistic flow rates (e.g., impact velocities ~180 m/s) and gas temperatures (1100°C). With the turbine specimens located at two different streamwise locations downstream of the combustor exit, the influence of gas temperature on deposition rate could be studied. It was noted that the upstream specimens (operating at gas temperatures ~1100°C) experienced one to two orders of magnitude higher deposition rates compared to the downstream specimens (operating at gas temperatures ~980°C). Compared to a previous series of tests with lower ash content (0.025%) residual fuel oil, the deposit levels with CWFs were two to three orders of magnitude larger for the same operating temperature. An aeroengine deposition study performed by Kim et al. with volcanic ash showed that the rate, at which deposition occurs, increases with time for a given turbine inlet temperature (TIT) and dust concentration, i.e., the vanes become better captors of material as the deposits on the vanes increase [5]. It was also found that once deposition begins, the mass of material deposited is proportional to dust concentration for a given TIT and dust exposure time.

Wenglarz and Fox [4] also explored the possibility of subcooling the upstream turbine specimens and found a factor of 2.5 reduction in deposits for a 200°C drop in metal surface temperature. Lower deposit formation in areas of reduced surface temperature was also noted by Bons et al. [6] in their study of serviced turbine hardware. Cooled turbine vanes, which exhibited large (1–2 mm thick) marine deposits over their entire surface, were noticeably free of deposits in the film cooling flow path where surface temperatures are significantly lower. This effect created substantial troughs or "furrows," which extended for more than ten hole diameters downstream of the cooling hole exit. These results confirm the important role of gas and surface temperature in determining deposition rates from ash-bearing fuels.

Due to current economic and political pressures, alternate fuels such as coal, petcoke, and biomass are being considered to produce substitute syngas fuels to replace natural gas in power turbines. Given the present volatility in natural gas markets and the uncertainty regarding projected fuel availability over the 20–30 year design lifetime of newly commissioned power plants, coal and petroleum derivative fuels are already being used at a

Contributed by the International Gas Turbine Institute (IGTI) of ASME for publication in the JOURNAL OF ENGINEERING FOR GAS TURBINES AND POWER. Manuscript received September 10, 2007; final manuscript received December 13, 2007; published online June 13, 2008. Review conducted by Dilip R Ballal.

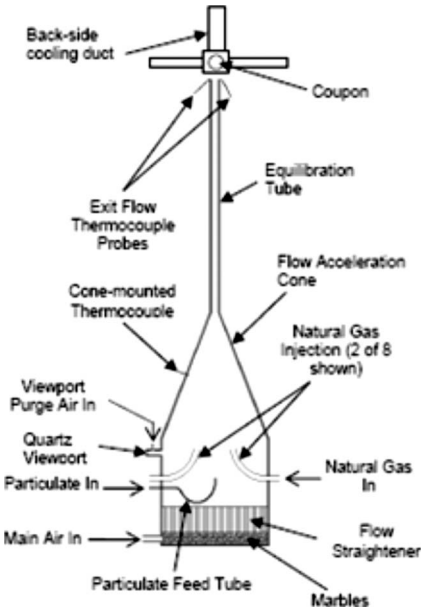

Fig. 1 BYU Turbine Accelerated Deposition Facility schematic

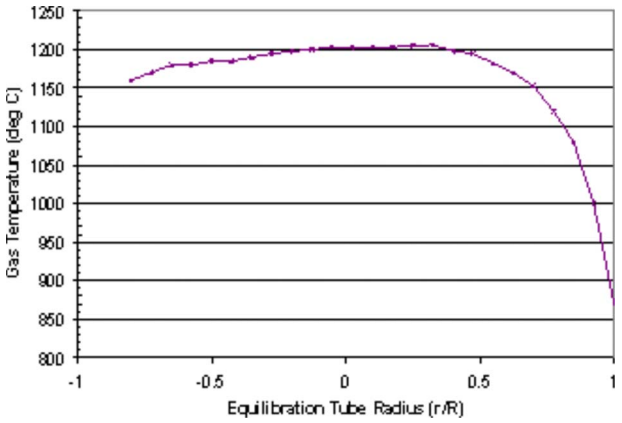

Fig. 2 Equilibration tube exit temperature profile for standard testing conditions (M=0.25 and T=1183°C)

handful of gas turbine power plants worldwide. In addition, intermediate goals of the DOE Future Gen and DOE Turbine Program focus on coal syngas as a turbine fuel in an effort to reduce dependency on foreign supplies of natural gas. Thus, the stage is set for broader integration of alternate fuels in gas turbine power plants. Studies of potential sources of deposition from these syngas fuels are necessary so that their adverse effects can be minimized. Deposition has numerous adverse results that can range from decreased engine performance to catastrophic failure of the blades. For monetary as well as safety reasons, it is highly desirable to reduce or eliminate these effects. In all but the most severe conditions, deposition is a relatively slow process and its study on an actual turbine is neither time nor cost efficient. To remedy this, an accelerated turbine facility has been developed, which simulates 8000 h of exposure time in a 4 h test. This is done by matching the net particle throughput mass at realistic combustor gas exit temperatures and velocities. The validation of this hypothesis was the subject of a previous paper by Jensen et al. [7]. Subsequently, this facility has been used to study alternate fuel deposition at constant operating conditions and the evolution of deposits with repeated exposure. The present study uses this facility to characterize the effects of deposition from coal- and petcoke-derived fuels on turbine blade materials as the particle size, gas temperature, and back side cooling level are varied independently.

Experimental Facility

Modifications. The Turbine Accelerated Deposition Facility (TADF) was originally built in 2004 (Fig. 1). Jensen et al. [7] described the facility in detail and provided validation of accelerated testing principles using airborne particulate. Its basic features include a partially premixed natural gas burning combustor capable of operating at an exit Mach number of 0.3 and an exit temperature of 1150°C, thus simulating the conditions at the entrance of a typical first stage nozzle guide vane for an F-class power generation turbine. One flow parameter that is not simulated is static pressure (deposition occurs at approximately atmospheric conditions). Jensen et al. cited a number of sources for facilities that also operate at lower pressures than an operating gas turbine engine and all concluded that particle temperature, concentration, and residence time are the critical parameters for proper simulation and not static pressure. A small fraction of the high pressure air is directed through a particle feed system, consisting of a syringe driven by a frequency controlled motor, which can be adjusted to yield the desired feed rate. Particulate from the syringe is entrained into the flow and enters at the base of the combustor. The particulate is then heated in the combustor and brought to thermal and velocity equilibrium in the 1 m long equilibration tube before impacting on a circular turbine blade specimen held at a desired impingement angle within one jet diameter of the tube exit.

Since its design, the TADF has been used for numerous deposition studies involving airborne particulate, biomass, coal, and petcoke [7–10]. In all previous studies, the fixture used to hold the test sample produced a nearly isothermal profile through the target specimen thickness. Modern engines employ significant internal and film cooling schemes to help protect blade materials. In order to more closely model these conditions, modifications were made to the TADF. Minor modifications to the combustor included: increasing the equilibration tube diameter to 2.54 cm to allow for a more uniform temperature profile and increasing the number of flame holders from 4 to 8 to maintain flame stability. The increase in tube diameter resulted in a slight decrease in exit velocity with the Mach number reduced to 0.25 for the operating temperature of 1183°C. Primary air flow was measured with a choked flow orifice to an uncertainty of ±3%. Figure 2 shows the temperature profile at standard test operating conditions (gas exit temperature =1183°C, Mach=0.25). The profile was measured by traversing a high temperature thermocouple probe across the lip of the tube exit. The thermocouple was not shielded and a radiation correction of 33°C at 1150°C was estimated using an emissivity of 0.5 for the oxidized Omegaclad™ probe surface. The thermocouple uncertainty was less than 15°C and the uncertainty in calculated Mach number was ±0.021.

The NASA Lewis chemical equilibrium code [11] was used to determine the composition of the combusted gas stream at 1183°C, based on the composition and flow rates of natural gas and air. For base condition in the TADF (1183°C, 0.0214 kg/s of inlet air, 0.000471 kg/s of inlet natural gas), the compositions of the combusted gas (in mol %) were 12.9% O_2, 3.8% CO_2, 7.2% steam, and the balance N_2.

A completely new specimen holder was designed to allow for impingement cooling (Fig. 3). Cool air is brought in through the center tube, impinges on the back side of the sample, and exits through the outer tube. The entire fixture is insulated with ceramic batting to minimize 3D heat transfer losses. When impingement cooling is used, the back side temperature of the sample is measured using two welded K-type thermocouples. Inlet and exit coolant temperatures are measured using K-type thermocouples as well. The sample's front side temperature is measured using a red-green-blue (RGB) camera through a technique described in the next section. A radiation shield helps vs minimize radiative

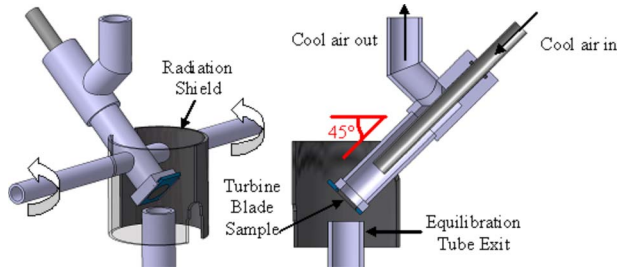

Fig. 3 Fixture designed to allow impingement cooling of turbine blade sample

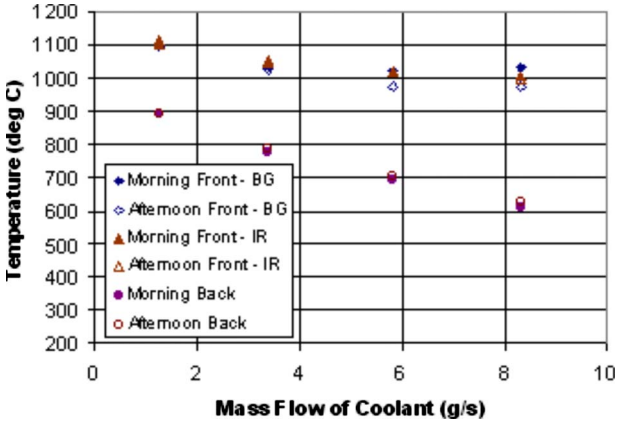

Fig. 4 Measured front side and back side temperatures as a function of cooling

losses while also providing optical access through a cutout (Fig. 3) for the RGB camera as well as digital video recording. The specimen holder can be rotated to hold the turbine sample at any impingement angle. All the tests in this study were conducted at 45 deg, as shown in Fig. 3, since this is representative of the leading edge stagnation region of a first stage vane. This impingement angle was found to produce the maximum surface degradation in tests conducted by Jensen et al. over a range of angles from 30 deg to 90 deg [7].

Three sets of circular turbine blade samples, all approximately 2.54 cm in diameter, were obtained from multiple industry sources for this study. In order to respect proprietary concerns of the manufacturers, strict source anonymity has been maintained for all data presented in this publication. The samples are representative of a high performance turbine material system: A nickel based superalloy substrate approximately 0.3 cm thick was common to all three sets, an MCrAlY bond coating approximately 225 μm thick for the first set, 200 μm for the second, and 175 μm for the third, and an air plasma sprayed (APS) yttrium stabilized zirconium (YSZ) thermal barrier coating (TBC) layer approximately 0.45 mm thick for the first set, 0.40 mm for the second, and 0.17 mm for the third. The samples were polished to a centerline average roughness (Ra) value of 1–1.5 μm.

Each of the three sets of coupons was used for a different test series, as will be explained in later sections; therefore, consistency for each test series was maintained. A small groove was machined around the circumference of each sample to allow it to be held in the cooling fixture with adequate sealing to contain the coolant. For all tests, pre- and post-test masses were measured as well as digital images taken. Uncertainty in the mass measurement is ± 5 mg. A Hommel T8000 profilometer was used for post-test measurements of the deposit surface roughness. Environmental scanning electron microscopy (ESEM) was employed as a post-test diagnostic to determine the extent of deposition and material system degradation. To prepare the samples for the ESEM, the samples were placed in epoxy, to preserve the deposit, cross sectioned, placed in Bakelite, and then polished.

During facility operation, the coupon front side surface temperature was measured with a Sony charge-coupled device (CCD) camera using a two-color technique based on previous work by Lu [12]. Figure 4 shows the variation in front side temperature as a function of coolant mass flow rate. The temperature uncertainty was estimated at 15.4°C. Back side temperatures from thermocouples welded to the back side of the coupon are also shown in the plot. The temperature difference between the front and back sides increases as the cooling flow rate increases, as expected, with temperature differences ranging from 200°C to 400°C. An additional front side temperature measurement was made with an IR thermometer. A surface emissivity of 0.2 was used to match the two-color temperature measurement for the lowest cooling rate. The IR temperature measurements seem to follow the average of the two-color measurements with this constant emissivity value. At the highest coolant flow rate indicated in the plot, the surface heat flux was estimated to be nearly 1000 kW/m^2 using a simple one-dimensional heat flow approximation—a value consistent with heat flux levels in modern first stage gas turbines.

Particulate Preparation. The coal and petcoke samples used in this study are the same as those described in Bons et al. [8], with the exception that the particle sizes have been substantially reduced. This was accomplished using a mechanical grinder with a collector to trap the particles exhausted out of the air filter. Subbituminous coal fly ash was obtained from an operating power plant, while the petcoke ash is boiler slag obtained from a combined cycle gas turbine power plant operating with a blend of 55% petcoke and 45% coal. The ash was characterized using an ESEM to perform X-ray spectroscopy, which can identify the elemental composition down to the atomic number of carbon. An independent elemental analysis was also conducted on the ash samples by ALS Chemex using inductively coupled plasma atomic emission spectroscopy (ICP-AES). The results were similar with only slight variation in the weight percentages of silicon, which were attributed to the ESEM measurements being spot measurements while the ICP-AES were bulk measurements.

To simulate ash that could be entrained by the flow leading to the turbine, the particles must be small enough to pass through the various gas cleanup systems. Filtration systems in modern gas turbine power plants are designed to remove all particles with diameters greater than 10 μm and a majority of particles larger than 1 μm. With inadequate or degraded filtration, these levels can be exceeded. This study focuses only on contamination from the fuel gas system. In addition to particles from the fuel stream, sand and dirt from the inlet air and rust from the gas turbine flow path can also form deposits resulting in spallation and TBC loss. This study is intended to supplement other studies performed by the authors, in which sand, biomass, and other synfuels have been used [7–10].

After grinding, the size of the ash samples was determined using the laser-based Coulter counter. The Coulter counter operates using a laser beam to illuminate the particles contained in a water slurry, which scatter light according to their size. Photodetectors convert the scattered light to particle size distributions. A more detailed explanation of the Coulter counter is given in Bons et al. [8]. Table 1 shows the particle size and elemental composition of the particulate used in the majority of the tests conducted in this study. The bulk density of each ash sample was measured in a graduated cylinder, and the apparent density (mass per particle exterior volume) was calculated using an estimated packing factor of 0.5.

Results and Discussion

Particle Size Series. Three series of tests were conducted to study the effects of particle size, gas exit temperature, and metal

Table 1 Ash particle summary statistics: size, density, and average elemental composition

	Coal	Petcoke
Mass mean diameter (μm)	3.1–16	6.3
Bulk density (g/cm^3)	0.99	1.45
Apparent density (g/cm^3)	1.98	2.90
Element	wt %	wt %
Na	6.9	4.3
Mg	3.6	2.2
Al	17.8	14.5
Si	47.4	38.3
P	1.6	0.0
S	1.8	1.0
K	2.6	2.5
Ca	8.7	7.5
Ti	1.6	0.8
V	0.0	3.4
Fe	6.4	22.9
Ni	0.0	0.9

temperature on deposition. The first test series looked at the effects of particle size on deposition. For the case of erosion, Hamed et al. [13] calculated the trajectories of various sizes of particles (10–50 μm) in a modern low pressure turbine (LPT) stage using a semiempirical particle rebound model. They found that larger particles actually have multiple rebounds between neighboring blades while smaller particles primarily impact the pressure surface only. To explore the effect of particle size on deposition, the present study used standard combustor operating conditions (gas exit temperature=1183°C, Mach=0.25) with the first set of 1 in. diameter turbine samples. The tests were run with no cooling air and the interior passage of the cooling fixture was insulated with blanket insulation material. The back side temperature was measured with two welded *K*-type thermocouples and found to be approximately 990°C, which is roughly 200°C below the combustor exit temperature.

Recently, Wammack et al. [9] conducted a deposition study using polished TBC turbine samples where the specimens were subjected to four consecutive testing cycles, returning the sample to room temperature between each test. They measured a significant increase in TBC surface roughness following the first thermal cycling. As a result, this roughened surface was much more susceptible to deposit accumulation compared to the highly polished surface prior to the first test cycle. To account for this effect in the current test series, an initial 1 h "burn-in" test was conducted with particulate injection, following which the combustor was shut down. The sample was allowed to cool without removing it from the fixture. Following this, the combustor was again brought to steady state and a standard 4 h test was conducted. Coal ash particulate was used in this test series, with four different sizes, each obtained from different locations in the mechanical grinder. The four particle size distributions (shown in Fig. 5) were obtained using the Coulter counter. The data shown in the figure are in wt %, so in all samples there are a majority of particles (by number) in the range below the mass mean diameter. ESEM images of the largest and smallest samples show a representative distribution of particle sizes (Fig. 6).

Using the pre-test and post-test mass measurements, the net specimen mass gain during exposure was assessed (Table 2). In some cases, the deposit was very fragile and much of it flaked off following the test as it cooled. The separated deposit percentage, defined as the amount of deposit that separated after the test ended divided by the net specimen mass gain, is also shown in the table. Percentages greater than 100% are indicative of significant spallation of the TBC layer where the mass of the separated deposit (plus TBC) weighed more than the net specimen mass gain. The

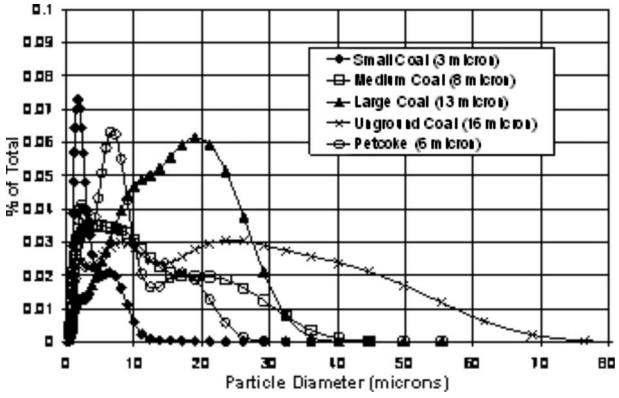

Fig. 5 Coal particle size distribution for four sizes tested

increasing percentage of separated deposit with increasing particle size indicates that TBC is more prone to spall with larger deposit formations.

Figure 7 shows two post-test images of the 13 μm particle test coupon. The first image was taken immediately after combustor shutdown while the second image was taken after the sample had cooled to room temperature. Streamwise aligned deposit structures are evident in the hot deposit image (Fig. 7(*a*)). These structures are similar to fuel deposit structures previously measured on a serviced turbine blade pressure surface by Bons et al. [6] (Fig.

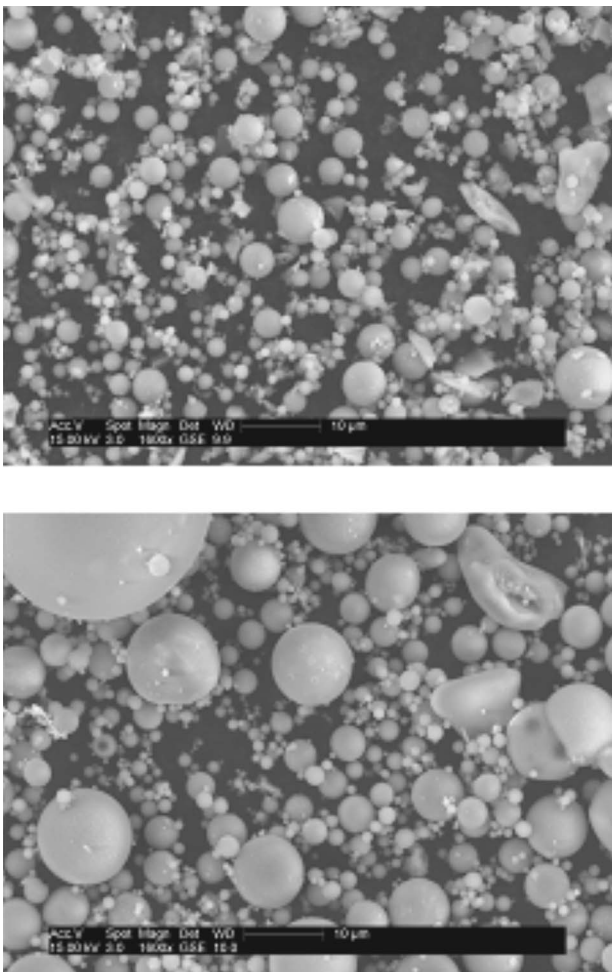

Fig. 6 ESEM images of smallest (top) and largest (bottom) size coal particles

Table 2 Deposition results from particle size test series

Particle size (μm)	Preburn button mass (g)	Button mass change (mg)	Separated deposit mass (mg)	Separated deposit (%)	Net deposit mass (mg)	Deposition rate (mg/cm^2 h)	Net particulate mass added to flow (mg)	Net capture efficiency (%)
3	14.73	70	300	81	370	14.6	10,050	3.68
8	14.88	60	450	88	510	20.13	10,350	4.93
13	14.12	−10	880	101	870	34.34	12,720	6.84
16	14.99	−140	1220	113	1080	42.63	13,390	8.07

8). The deposits in Fig. 8 were considerably more tenacious than the accelerated coal deposits in this case, since they were still intact on the blade surface after cooldown. With rapid cooling, the mismatch in thermal expansion coefficients between the metal, the TBC, and the deposit results in the removal of most of the deposit with some of the TBC as well. TBC spallation is evident primarily along the leading edge of the circular specimen (Fig. 7(*b*)), even though the deposit thickness is approximately uniform over the entire coupon (Fig. 7(*a*)). Wammack et al. observed similar behavior in their deposition tests and attributed this to the impingement of deposit-laden gas at the exposed metal/TBC interface [8]. Thus, material system degradation (e.g., TBC spallation) was always most significant at the leading edge of the turbine specimen. In a gas turbine, similarly exposed TBC/metal interfaces are evident at each of the film cooling holes in the stagnation region of the blade. This explains the common occurrence of TBC spallation adjacent to stagnation film holes as described by Bons et al. [6]. The extent of spallation and material system degradation will be discussed further using ESEM images.

Dividing the net deposit mass by the exposed coupon surface area and the test duration yielded deposition rate measurements from 14 mg/cm^2 h to 43 mg/cm^2 h for the smallest and largest size particles (Table 2). Figure 9 shows the effect of particle size on net capture efficiency (mg/h of deposit divided by mg/h of particulate added to the flow). Capture efficiency increases asymptotically with particle size with a more than 50% increase from 3 μm to 16 μm. These results suggest that with filter degradation, deposition problems as well as turbine hardware damage are likely to increase considerably. Additionally, it is important to note that even the smallest size particles tested showed significant deposition. This would indicate that even with properly functioning filtration systems, the problems associated with deposition and spallation cannot be entirely eliminated. These deposition rates are lower than previous measurements in the same facility reported by Bons et al. (70–140 mg/cm^2 h) and those reported by Wenglarz and Fox (200–400 mg/cm^2 h) [7,4]. This may be due to the lower particulate loadings used in the present study compared to Bons et al. [8] (less than 100 ppmw h versus 150–600 ppmw h, respectively).

Despite the larger particle size and increased capture efficiency, roughness measurements of the deposit surface did not show a significant trend with particle size. Four 15 mm long profilometer traces were made on each coupon following the combustor shutdown. Loose deposits that flaked off during cooldown were not evaluated for this assessment. Roughness statistics taken from these four residual deposit measurements were averaged to yield typical values for each coupon. While the residual deposit surfaces were considerably more rough (Ra$\cong$7 μm and Rt $\cong$50 μm) than the pre-test coupon surface (Ra$\cong$1 μm), average roughness values for the 3 μm and 16 μm particles were approximately the same.

Gas Temperature Series. The second test series was performed using coal ash with a mass mean diameter (MMD) of 3 μm with no cooling air and the interior of the coolant passage still insulated. Six tests were performed at five different gas exit temperatures using the second set of samples. Two of the tests were performed at a gas exit temperature of 1183°C, which is typical in many modern first stage gas turbine engines while the other tests were at lower temperatures. All of the tests experienced a nominal particulate loading of 96 ± 12 ppmw h. This loading is intended to simulate an engine operating for one year (8000 h) at a low particulate concentration of 0.01 ppmw. This standardization of ppmw h has been used previously [7–9] to simulate long

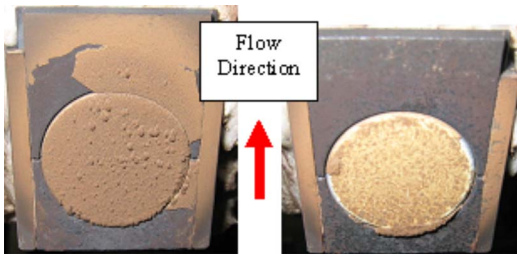

Fig. 7 Post-test images of coupon subjected to 13 μm particle size

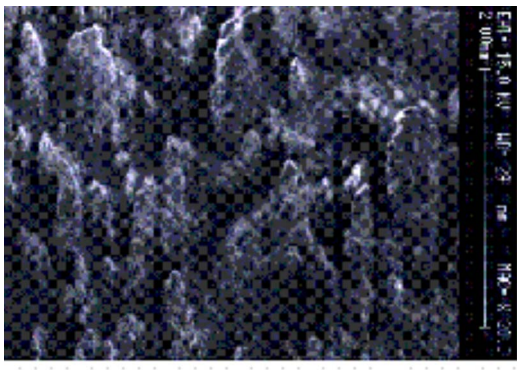

Fig. 8 Micrograph image taken of turbine blade pressure surface deposits (flow direction is bottom to top)

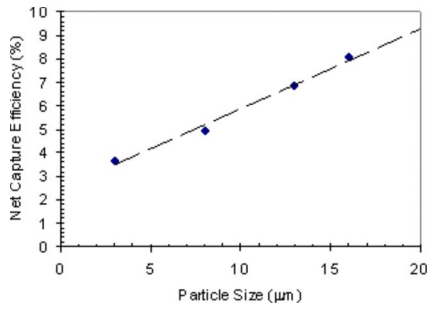

Fig. 9 Effect of particle size on net capture efficiency

Table 3 Deposition results from gas temperature test series

Gas temperature (°C)	Preburn button mass (g)	Button mass change (mg)	Separated deposit mass (mg)	Separated deposit (%)	Net deposit mass (mg)	Deposition rate (mg/cm^2 h)	Net particulate Mass (mg)	Net capture efficiency (%)
1183	13.66	40	100	71	140	6.91	7880	1.78
1183	13.66	40	110	73	150	7.4	8220	1.82
1074	13.64	60	0	0	60	2.96	7590	0.79
1020	13.64	30	0	0	30	1.48	7820	0.38
966	13.69	10	0	0	10	0.49	7360	0.14
860	13.62	0	0	0	0	0	7860	0

duration turbine operation. A similar metric was used by Caguiat [14], in which accelerated compressor fouling caused by salt water ingestion was studied. By using this metric, the results can be interpreted to a wide range of applications. Airflow was adjusted to maintain an exit velocity of 170 m/s for each test, which at the gas temperatures tested yielded Mach numbers ranging from 0.23 to 0.26. Since the mode of deposition for particles on the order of 3 μm is inertial impaction, this constant jet velocity condition maintains the same kinetic energy at particle impact. Accordingly, the only relevant variable in this test series is the particle temperature, which was calculated to be in thermal equilibrium with the gas at the exit of the 1 m long equilibration tube. Once the facility reached steady state, particle seeding commenced and lasted for 4 h, after which the facility was immediately shut down. The initial 1 h burn-in test was not performed for this test series.

Deposits were very similar to the 3 μm test from the particle size series. The same flaking was observed for the tests run at 1183°C, but very little flaking was noticed at lower temperatures. Deposition results are summarized in Table 3. Repeated tests were run at an exit temperature of 1183°C to show the repeatability of the facility. The deposition rate decreased by approximately 58% with the first 100°C drop in gas temperature. This was followed by another 50% decrease with an additional 50°C drop. An additional 50°C drop in gas temperature to 966°C resulted in a 67% decrease in deposition rate. At 860°C, no deposit formed indicating a gas temperature threshold for deposition around 960°C for this study. This compares well with studies performed previously by Wenglarz and Fox using coal-derived fuel, Kim et al. using volcanic ash, and Jensen et al. using airborne dust. Since these gas temperatures are all lower than the melting temperature of the ash compounds, the rising deposition rate with gas temperature is likely due to the increased tendency for deposit sintering at elevated temperatures. Sintering creates large deposit masses that are less susceptible to removal by erosion from subsequent particle impacts. Figure 10 shows the corresponding decrease in net capture efficiency with gas temperature. It is noted that the capture efficiency at 1183°C in Fig. 10 is approximately 50% of that shown in Fig. 9 for the same 3 μm particle size. This is due to the effect of the burn-in, which was not performed for this test series.

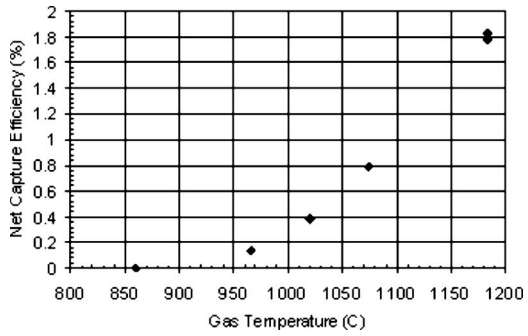

Fig. 10 Effect of gas temperature on net capture efficiency

Figures 11(*a*)–11(*c*) show digital images of specimens at 1183°C, 1074°C, and 966°C. Note the large amount of separated deposit for the high temperature case and the lack of substantial deposits at low temperature (though the coupon is still discolored at the lower edge near jet impact). Based on the trend in Fig. 10, we would expect deposition rates to increase for G- and H-class engines, which operate above 1500°C. However, some of the constituents may be in a vapor phase at these temperatures so the degree to which deposition would increase might not be exponential, as indicated in Fig. 10. The authors are unaware of any deposition tests in the open literature that operate at higher temperatures than those in this study.

A similar trend with gas temperature is noted in the deposit roughness measurements shown in Fig. 12. All three statistical roughness metrics (centerline average [Ra], average peak height [Rz], and peak height [Rt]) increase as gas temperature is increased above the deposition threshold temperature of 960°C. It should be noted that due to extensive deposit flaking at 1183°C, the roughness measurement shown in Fig. 12 is actually taken from a separated flake of deposit rather than from the residual deposit on the coupon surface.

The strong dependency of deposition rate on gas (and particle) temperature has important implications for modern turbine blade rows where the gas temperature can drop by 150–250°C per stage. If the turbine inlet temperature is high enough so that particles are molten or sinter readily, they may collect primarily near the leading edge—since with falling temperatures through the

Fig. 11 Digital images of postburn coupons at (from left to right) 1183°C, 1074°C, and 966°C

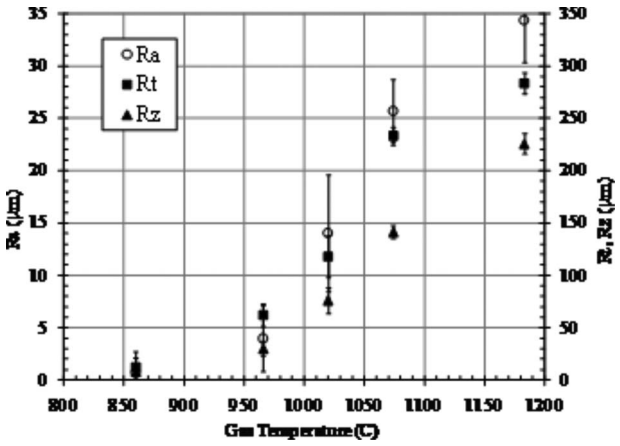

Fig. 12 Effect of gas temperature on deposit roughness

Table 4 Deposition results from impingement cooling test series using coal

Mass flow of coolant (g/s)	Heat flux (kW/m^2)	Preburn button mass (g)	Button mass change (mg)	Separated deposit mass (mg)	Separated deposit (%)	Net deposit mass (mg)	Deposition rate ($mg/cm^2 h$)	Net particulate mass (mg)	Net capture efficiency (%)
0	0	14.73	70	300	81	370	14.6	10050	3.68
1.26	500.68	30.56	130	90	41	220	8.68	8480	2.59
3.38	1049.21	30.69	120	20	14	140	5.53	9270	1.51
5.81	1404.35	30.53	100	0	0	100	3.95	8120	1.23
8.33	1614.26	30.93	0	0	0	0	0	9540	0

vane passage, sintering may no longer be possible. If, however, the gas temperature at the vane inlet is so high that corrosive elements are in the vapor phase, then they may not deposit on the vane. Rather, they may wait until the temperature drops and then begin to condense on the surface—perhaps in the subsequent blade row. Another factor affecting deposit buildup is of course the flow angle relative to the local surface. The flow is directly impinging at the leading edge, whereas it is mostly parallel to the wall at midspan.

Impingement Cooling Series. The third test series was performed to study the effects of impingement cooling on deposition. The insulation was removed from the interior of the cooling fixture and two *K*-type thermocouples were welded to the back side of each sample to measure the back side temperature. This test series used the same set of samples as in the particle size series. The RGB camera was used to measure the sample front side temperature and two *K*-type thermocouples were used to measure the incoming and outgoing coolant temperatures. Four tests were run at varying mass flows of coolant. The same coal ash was used as in the gas temperature series (3 μm diameter) and the standard combustor operating conditions, as used in the particle size series, were used including the initial 1 h burn-in test. All of the tests experienced a nominal particulate loading of 110 ± 7 ppmw h, only slightly higher than the gas temperature series due to the additional 1 h burn-in test.

The deposits formed in this test series were much more tenacious than the previous ones. Appreciable deposit flaking was only observed for the 1.26 g/s cooling case and it was minimal. This result is consistent with the behavior of the gas temperature series, in which the lower gas temperatures showed a more tenacious deposit. The applied coolant lowers the temperature of the TBC surface producing a thinner deposit layer. Thin deposit layers are not as susceptible to flaking induced by thermal contraction during cooldown. Table 4 provides a summary of the deposition results. The deposition rate was reduced by approximately 40% with the initial level of cooling. This was followed by further reductions as the amount of cooling was increased. Corresponding trends in net capture efficiency are shown in Fig. 13. For this series, spallation occurred, but was limited to very small portions of the edge at the base of the sample. The amount of visible spallation decreased slightly with increased coolant mass flow. The drop in capture efficiency noted in Fig. 13 is similar to the result of Wenglarz and Fox [4] who observed a factor of 2.5 reduction in deposits for a 200°C drop in metal surface temperature produced by subcooling. The present results show a factor of 4 reduction in deposits for a 360°C drop in back side temperature (100°C drop in front side temperature—see Fig. 4) with cooling. These results clearly show the benefits of cooling in reducing deposition. However, in G- and H-class engines, the amount of cooling needed to obtain the necessary drop in front side temperature could be prohibitive. These results also suggest that film cooling could provide an additional reduction in deposition and spallation. However, Bons et al. [6] noted that film cooling holes introduce exposed TBC/metal interfaces that are actually more prone to spallation.

To further assess the level of TBC degradation, the test articles from this test series were analyzed using the ESEM. The cross sectioned samples were first used to measure the thickness of deposit remaining on the surface (Fig. 14). Three images were taken of the cross sectioned sample: one at the bottom of the sample (closest to the combustor exit), one near the middle, and one at the top. Figure 15 shows a typical series of images taken from the 5.81 g/s cooling level sample.

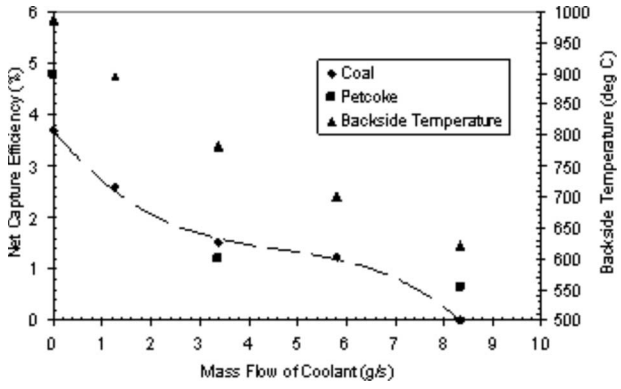

Fig. 13 Effect of cooling on net capture efficiency

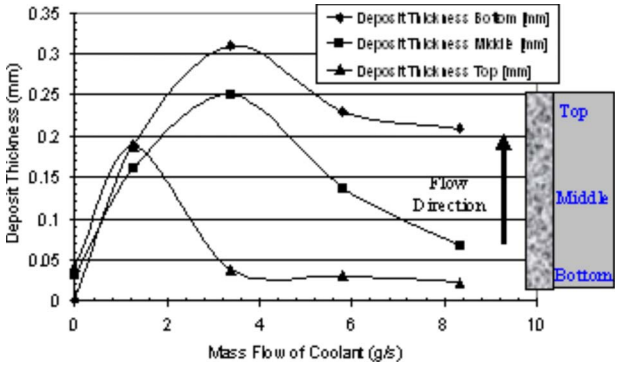

Fig. 14 Remaining deposit thickness versus cooling level

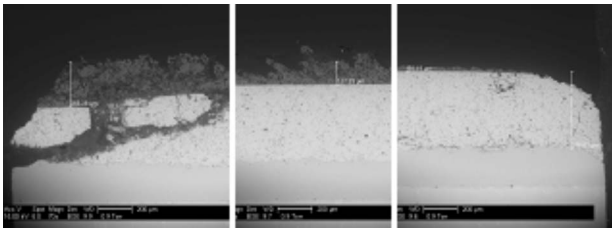

Fig. 15 Typical image series of bottom (left), middle, and top (right) portions of 5.81 g/s coolant test sample

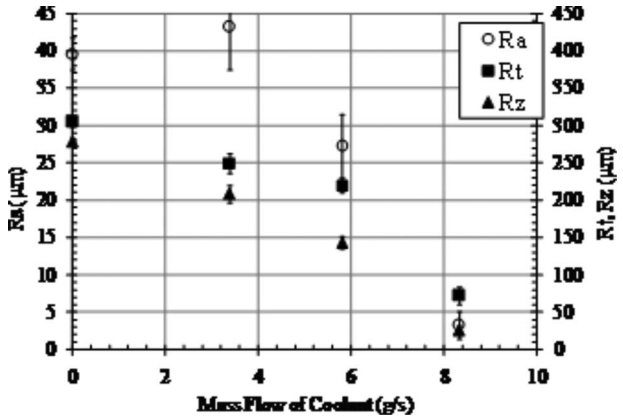

Fig. 16 Effect of cooling on deposit surface roughness

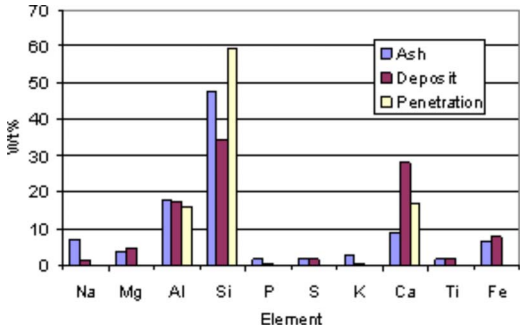

Fig. 17 Elemental comparison of ash, deposit, and penetration for coal impingement cooling series

As seen in Fig. 14, residual deposit thickness is fairly uniform for the no cooling and lowest level of cooling cases. This is indicative of the large percentage of separated deposit for these two cases as noted in Table 4. As the amount of cooling was increased to 3.3 g/s, the top deposit thickness dropped off considerably while the middle and bottom continued to increase because of the more tenacious deposit formation near the leading edge. Since the top of the coupon was furthest from the jet, it experienced the lower temperatures and thus less deposition. Further increases in the amount of coolant result in decreasing deposit thicknesses at all locations. This spatial variation in deposit thickness is similar to what occurs in an actual turbine with deposition buildup at the hottest spots near the leading edge [6]. Figure 15 shows the level of spallation, which occurred at the leading edge as a result of deposit penetration. Similar spallation was seen in the particle size test series. Wammack et al. [9] observed a similar deposit penetration effect although with a different TBC material system. With the exception of the highest cooling case, all other tests in this series had varying amounts of spallation damage caused by penetration of the deposit along the cross section.

Figure 16 contains the surface roughness data for the impingement cooling test series. As expected, the roughness falls off as the deposit is reduced due to increased back side cooling. The roughness measurement for the no cooling case was taken from a separated deposit flake to ensure consistency with the more tenacious deposits at the higher cooling levels.

X-ray spectroscopy was conducted to determine the elemental constituents in the surface deposit, as well as the penetrating deposits. Figure 17 shows the elemental composition in wt % compared with the ash. The surface deposits showed a similar makeup as the ash; however, there was a significant increase in Ca while Na and Si showed large decreases. The figure also clearly shows that the TBC studied is penetrated by Si, Ca, and Al from the ash. The spallation appears to be the result of the difference in coefficients of thermal expansion between the TBC and the penetrating ash elements. Upon shutdown of the facility, this mismatch in contraction rates causes significant thermal stresses in the TBC, resulting in separation of the TBC layer particularly near the edges of the coupon.

Petcoke Series. A final series of tests were performed using the petcoke/coal blend particulate. Three tests were conducted using particles with a MMD of 6 μm. The third set of samples described earlier was used in this test series. First, a no cooling test was performed with the interior of the coolant fixture insulated as in the gas temperature and particle size test series. Following this, two impingement cooling levels were tested in the same configuration as the coal series. The same standard operating conditions were used, namely, $T=1183\,^{\circ}\mathrm{C}$, Mach=0.25. The deposits looked similar to those of the coal impingement cooling series. The same large amount of flaking occurred on the no cooling case; however, there was more flaking on the cooling cases compared to the coal series perhaps due to the larger particle size. There was slightly more spallation of the TBC in the no cooling case compared to the coal; however, the different MMD makes a direct comparison difficult. A summary of the deposition results is shown in Table 5. Trends in net capture efficiency are included in Fig. 13 with the coal.

Conclusions

Four series of tests were performed in an accelerated deposition test facility to study the independent effects of particle size, gas temperature, and metal temperature on ash deposits from two candidate power turbine synfuels. Testing was conducted in the TADF by matching gas temperature, velocity, and net throughput of particulate out of the combustor with that experienced by a modern power turbine. Nominal combustor exit flow conditions are Mach number of 0.25 and gas temperature of $1183\,^{\circ}\mathrm{C}$. Testing with four different sizes of coal ash particles showed greater than double the deposition rate as particle mass mean diameter was increased from 3 μm to 16 μm. In the second series of tests, different gas temperatures were studied while the facility maintained a constant exit velocity of 170 m/s (Mach=0.23–0.26). Particle deposition rate was found to decrease with decreasing gas temperature. The threshold gas temperature for deposition was approximately $960\,^{\circ}\mathrm{C}$. Ground coal and petcoke ash particulates were used in the third and fourth test series with impingement cooling on the back side of the target coupon. Deposition rates decreased with increasing mass flow of coolant air, as expected. Deposit surface roughness levels decreased with decreasing gas

Table 5 Deposition results from impingement cooling test series using petcoke

Mass flow of coolant (g/s)	Heat flux (kW/m^2)	Preburn button mass (g)	Button mass change (mg)	Separated deposit mass (mg)	Separated deposit (%)	Net deposit mass (mg)	Deposition rate ($mg/cm^2\,h$)	Net particulate mass (mg)	Net capture efficiency (%)
0	0	13.8	10	360	97	370	14.60	7720	4.79
3.38	1049.20	29.4	40	60	60	100	3.95	7680	1.22
8.33	1614.26	29.42	20	30	60	50	1.97	8200	0.65

temperature and increasing coolant flow, consistent with the trend in particulate capture efficiencies for both cases. Postexposure analyses of the third test series (scanning electron microscopy and X-ray spectroscopy) show decreasing TBC damage with increased cooling levels. Work is currently under way to study the effects of different TBC application techniques on deposition.

Acknowledgment

Various individuals provided invaluable support to this research effort. The authors would particularly like to thank the assistance provided by Arun Mehta from Pacificorp for the coal flyash samples and Tampa Electric Company for assistance in locating petcoke samples. Dr. Ron Bunker of GE, Mr. Gerry McQuiggan of Siemens-Westinghouse, and Dr. Tom Taylor of Praxair Surface Technologies all generously donated coupon specimens without which the study would not have been possible. Thanks also to Robert Laycock for performing particle size analysis and many other helpful tasks. Aaron Mason and Spencer Grange helped us design the coolant fixture and conduct testing. A special thanks to Ken Forster, projects laboratory manager for the M.E. Department at Brigham Young University; without his help, this project would not have been possible. This work was partially sponsored by the US Department of Energy—National Energy Technology Laboratory through a cooperative agreement with the South Carolina Institute for Energy Studies at Clemson University.

Nomenclature

M = Mach number
Q = heat flux (W)
Ra = centerline average roughness
Rt = peak roughness
Rz = average peak roughness
T = temperature
c_p = specific heat at constant pressure (J/kg K)
m = mass flow rate (kg/s)

References

[1] Wenglarz, R. A., and Wright, I. G., 2002, "Alternate Fuels for Land-Based Turbines," *Proceedings of the Workshop on Materials and Practices to Improve Resistance to Fuel Derived Environmental Damage in Land-and Sea-Based Turbines*, Oct. 22–24, Colorado School of Mines, Golden, CO.
[2] Smialek, J. L., Archer, F. A., and Garlick, R. G., 1992, *The Chemistry of Saudi Arabian Sand: A Deposition Problem on Helicopter Turbine Airfoils* Advances in Synthesis and Processes, SAMPLE, 3, pp. M92–M101.
[3] Toriz, F. C., Thakker, A. B., and Gupta, S. K., 1988, "Thermal Barrier Coatings for Jet Engines," presented at the Gas Turbine and Aeroengine Congress Amsterdam, The Netherlands, June 6–9, Paper No. 88-GT-279.
[4] Wenglarz, R. A., and Fox, Jr., R. G., 1990, "Physical Aspects of Deposition From Coal-Water Fuels Under Gas Turbine Conditions," ASME J. Eng. Gas Turbines Power, **112**, pp. 9–14.
[5] Kim, J., Dunn, M. G., Baran, A. J., Wade, D. P., and Tremba, E. L., 1993, "Deposition of Volacanic Materials in the Hot Sections of Two Gas Turbine Engines," ASME J. Eng. Gas Turbines Power, **115**, pp. 641–651.
[6] Bons, J. P., Taylor, R., McClain, S., and Rivir, R. B., 2001, "The Many Faces of Turbine Surface Roughness," ASME J. Turbomach., **123**, pp. 739–748.
[7] Jensen, J. W., Squire, S. W., Bons, J. P., and Fletcher, T. H., 2005, "Simulated Land-Based Turbine Deposits Generated in an Accelerated Deposition Facility," ASME J. Turbomach., **127**, pp. 462–470.
[8] Bons, J. P., Crosby, J., Wammack, J. E., Bentley, B. I., and Fletcher, T. H., 2007, "High Pressure Turbine Deposition in Land-Based Gas Turbines With Various Synfuels," ASME J. Eng. Gas Turbines Power, **129**, pp. 135–143.
[9] Wammack, J. E., Crosby, J., Fletcher, D., Bons, J. P., and Fletcher, T. H., 2006, "Evolution of Surface Deposits on a High Pressure Turbine Blade—Part I: Physical Characteristics," ASME J. Turbomach., **130**, p. 021020.
[10] Bons, J. P., Wammack, J. E., Crosby, J., Fletcher, D., and Fletcher, T. H., 2006, "Evolution of Surface Deposits on a High Pressure Turbine Blade—Part II: Convective Heat Transfer," ASME J. Turbomach., **130**, p. 021021.
[11] McBride, B. J., and Gordon, S., 2006, "Computer Program for Calculation of Complex Chemical Equilibrium Compositions and Applications II. User's Manual and Program Description," http://www.grc.nasa.gov/WWW/CEAWeb/RP-1311P2.htm.
[12] Lu, H., 2006, "Experimental and Modeling Investigations of Biomass Particle Combustion," Ph.D. dissertation, Chemical Engineering Department, Brigham Young University, Provo, UT.
[13] Hamed, A., Tabakoff, W., Rivir, R. B., Das, K., and Arora, P., 2004, "Turbine Blade Surface Deterioration by Erosion," ASME Paper No. GT2004-54328.
[14] Caguiat, D., 2002, "Rolls Royce/Allison 501-K Gas Turbine Anti-Fouling Compressor Coatings Evaluation," ASME Paper No. GT2002-30261.